An Equivalent Circuit Model of Passively Mode-Locked Hybrid Silicon Laser

Mohammad Shekarpour and Mohammad Hasan Yavari, *Member, IEEE*

***Abstract*— In this letter, for the first time, we present a circuit-level model (CLM) of semiconductor mode-locked laser (MLL) based on delay differential equation (DDE). To confirm that our model is valid for different structures, the CLM of the hybrid silicon MLL is analysed for the cases without and with an intracavity filter. The ability of CLMs to replicate dynamic behavior of repetition rate is demonstrated. Furthermore, the effect of linewidth enhancement factor (LEF) on pulse width and peak power is investigated. The presented model simulates transition from mode-locking to chaotic regime by changing LEF, rigorously. The results of CLM are in good agreement with numerical and experimental results reported in other works. By a versatile procedure introduced in this letter for CLM, different type of MLLs based on DDE can be developed.**

***Index Terms*— Semiconductor lasers, mode-locked lasers, circuit level model.**

I. Introduction

SEMICONDUCTOR MLLs as a mechanically stable and short pulse sources offer high repetition rates [1], and are well suited for high bit-rate optical communication systems [2]. Lots of works have been done on the experimental [3]–[8], theoretical [9]–[12] and numerical modeling [13]–[21] of MLLs, in which internal physical mechanisms are described in great detail. With regards to the fast growing complexity and size of photonic integrated circuits (PICs) [22], especially silicon based PICs due to their compatibility with CMOS technology, the computer-aided design (CAD) is required for developing large optoelectronic systems. Considering important role of MLLs in PICs, the effective design incorporating MLLs requires appropriate model. The numerical model of MLL based on finite difference traveling wave is accurate [14]–[16], however, it is computationally intensive. This feature makes it unattractive for the CAD tools. To the best of our knowledge, for the first time, this letter describes a circuit-level implementation of MLLs.

In this work, the accurate CLM of MLL is developed based on DDE for without-intracavity structure (WOICS) and with-intracavity structure (WICS). Also the influence of intracavity and LEF on the dynamic behavior of passively mode-locked hybrid silicon lasers are investigated and validated by numerical results of DDE model.

Manuscript received January 24, 2022; revised March 10, 2022; accepted May 5, 2022. Date of publication May 16, 2022; date of current version May 23, 2022. *(Corresponding author: Mohammad Hasan Yavari.)*

The authors are with the Faculty of Engineering, Shahed University, Tehran 3319118651, Iran (e-mail: mohammad.shekarpour@shahed.ac.ir; mh.yavari@shahed.ac.ir).

Color versions of one or more figures in this letter are available at https://doi.org/10.1109/LPT.2022.3175410.

Digital Object Identifier 10.1109/LPT.2022.3175410

II. DDE Model of WOICS and WICS

Fig. 1(a) and (b) show the ring lasers for WOICS and WICS proposed in [7]. Based on the models proposed in [13], [18], [19], [20], in this letter we extend the DDE model to study harmonic mode-locking (HML) of the long cavity lasers as shown in Fig. 1. Equations (1) and (2) describe the slowly varying field amplitude E in WOICS and WICS, respectively. In (2), intracavity filter is introduced by coupling the laser cavity to the passive cavity. The final set of three coupled DDEs for the slowly varying field amplitude E, the saturable gain G and the saturable loss Q are

$$\gamma^{-1}\dot{E}(t) = -E(t) + R_0(t-T_0)e^{-i\Delta\Omega T_0}E(t-T_0) \tag{1}$$

$$\gamma^{-1}\dot{E}(t) = -E(t) + R_1(t-T_0)e^{-i\Delta\Omega T_0}E(t-T_0) + \sum_{l=1}^{\infty} e^{-ilc-i\Delta\Omega(T_0+l\tau)}R_{l+1}(t-T_0-l\tau) \times e^{-i\Delta\Omega(T_0+l\tau)} \times E(t-T_0-l\tau) \tag{2}$$

$$\gamma_g^{-1}\dot{G}(t) = \gamma_g^{-1}J_g - G(t) - \gamma_g^{-1}e^{-Q(t)}(e^{G(t)}-1)|E(t)|^2 \tag{3}$$

$$\gamma_q^{-1}\dot{Q}(t) = \gamma_q^{-1}J_q - Q(t) - \gamma_q^{-1}r_s e^{-Q(t)}(e^{Q(t)}-1)|E(t)|^2 \tag{4}$$

$$R_m(t) = \sqrt{k_m}e^{1/2(1-i\alpha_g)G(t)-1/2(1-i\alpha_q)Q(t)} \quad m=0,1,2,3 \tag{5}$$

where (1), (3) and (4) model the WOICS and (2), (3) and (4) model the WICS. J_g is unsaturated gain and J_q is unsaturated absorption. The carrier lifetimes in the gain and absorber sections are given by $1/\gamma_g$ and $1/\gamma_q$, respectively. The factor r_s is proportional to the ratio of the saturation energies in the gain and absorber sections. T_0 is the cold cavity roundtrip time for the configuration WOICS and WICS. τ is the cold cavity roundtrip time for intracavity filter. The bandwidth of the laser is taken into account by a Lorentzian-shaped filter function with full-width at half maximum (FWHM) γ. Here l is the number of roundtrips in intracavity filter and c is the phase of the light due to one roundtrip in the intracavity filter. $\Delta\Omega$ accounts for a possible detuning between the frequency of the maximum of the gain spectrum and the frequency of the nearest cavity mode. The LEF in the gain and absorber sections are denoted by α_g and α_q, respectively. Spontaneous emission is modeled in (1) and (2) by a complex Gaussian white-noise term $\xi(t)$ with strength D. In (5), $R_i(t)$ describes the amplification and losses of the field during roundtrip in the

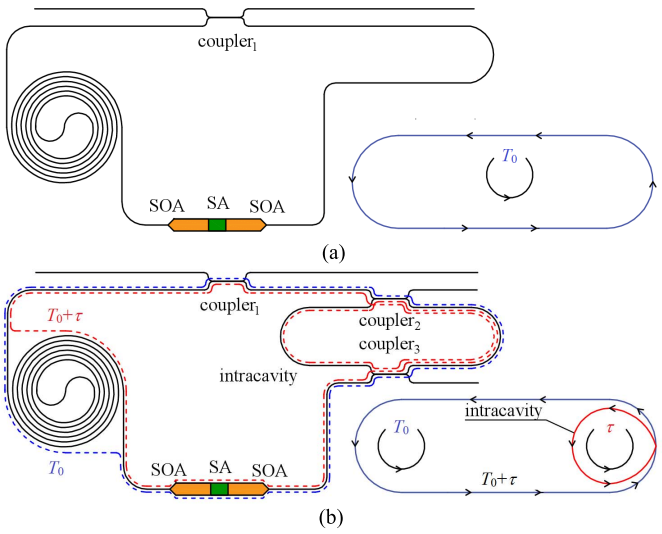

Fig. 1. Schematic of (a) WOICS and (b) WICS [7], [18], [19]. Left: the structures are implemented on silicon substrate. Right: corresponding paths for time delays used for derivation of DDE model.

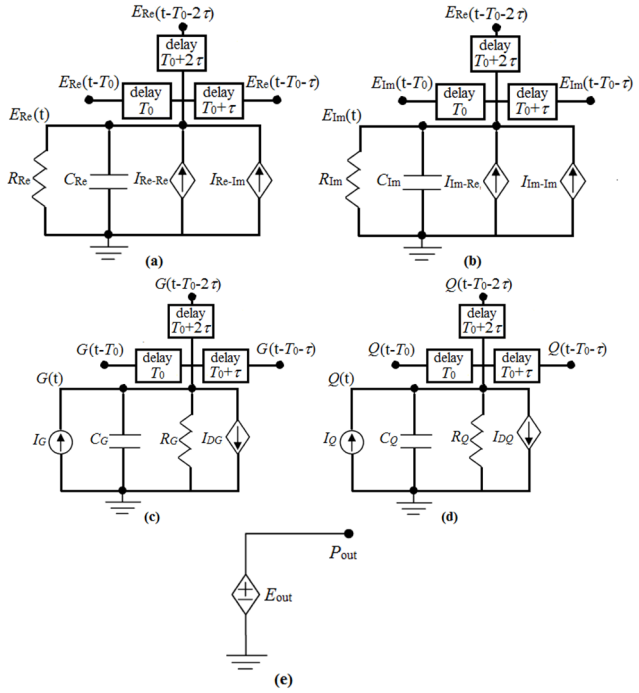

Fig. 2. Circuit-level implementation of WICS.

ring cavity. As shown in Fig. 1, the delay time of WOICS is T_0 and for WICS assuming $l = 2$, the DDE is based on three delay time T_0, $T_0+\tau$ and $T_0+2\tau(\tau = 0.1T_0)$. The parameters for the simulations are given in [7], [14], [17], [18], [19], [20].

III. Circuit Model Implementation

Due to the existence of complex exponential terms in (1) and (2), in order to convert these equations into a form that can be modeled by lumped circuit elements, E is separated into a real and imaginary parts as:

$$E(t) = E_{\mathrm{Re}}(t) + jE_{\mathrm{Im}}(t) \tag{6}$$

By substituting (6) into (2) and assuming $l = 2$, we obtain

$$\begin{aligned}
&\gamma^{-1}\dot{E}_{\mathrm{Re(Im)}}(t)\\
&\quad = -E_{\mathrm{Re(Im)}}(t) + \sqrt{k_1}e^{1/2(G(t-T_0)-Q(t-T_0))}\\
&\qquad \times (E_{\mathrm{Re(Im)}}(t-T_0)\cos(W_1(t-T_0))\\
&\qquad + (-)E_{\mathrm{Im(Re)}}(t-T_0)\sin(W_1(t-T_0)))\\
&\qquad + \sqrt{k_2}e^{1/2(G(t-T_0-\tau)-Q(t-T_0-\tau))}\\
&\qquad \times (E_{\mathrm{Re(Im)}}(t-T_0-\tau)\cos(W_2(t-T_0-\tau))\\
&\qquad + (-)E_{\mathrm{Im(Re)}}(t-T_0-\tau)\sin(W_2(t-T_0-\tau)))\\
&\qquad + \sqrt{k_3}e^{1/2(G(t-T_0-2\tau)-Q(t-T_0-2\tau))}\\
&\qquad \times (E_{\mathrm{Re(Im)}}(t-T_0-2\tau)\cos(W_3(t-T_0-2\tau))\\
&\qquad + (-)E_{\mathrm{Im(Re)}}(t-T_0-2\tau)\sin(W_3(t-T_0-2\tau)))\ l=2\\
&W_1(t) = 0.5\times(\alpha_g G(t) - \alpha_q Q(t) + 2\Delta\Omega T_0)\\
&W_2(t) = 0.5\times(\alpha_g G(t) - \alpha_q Q(t) + 2\Delta\Omega(T_0+\tau) + c)\\
&W_3(t) = 0.5\times(\alpha_g G(t) - \alpha_q Q(t) + 2\Delta\Omega(T_0+2\tau) + 2c)
\end{aligned} \tag{7}$$

It is noted that when the optical field does not pass through the intracavity, the delay time is T_0 and if the field passes through the intracavity, delay times are $T_0 + \tau$ and $T_0 + 2\tau$. To model the separated equation (7), E_{Re} and E_{Im} are considered as node voltages. Thus, resistors $R_{\mathrm{Re}} = R_{\mathrm{Im}} = 1$ represent the first term of right side of (7). Also, the terms related to the time derivation of optical field are modeled by capacitors $C_{\mathrm{Re}} = C_{\mathrm{Im}} = \gamma^{-1}$. In this equation, terms that include time-delayed optical field $E_{\mathrm{Re(Im)}}(t-T_0)$, $E_{\mathrm{Re(Im)}}(t-T_0-\tau)$ and $E_{\mathrm{Re(Im)}}(t-T_0-2\tau)$, are modeled by current dependent sources, because they depend on $E_{\mathrm{Re(Im)}}$. Also, since the field is separated into real and imaginary parts, the related current dependent sources are as follows:

$$\begin{aligned}
&I_{\mathrm{Re-Re(Im-Im)}}\\
&\quad = \sqrt{k_1}e^{1/2(G(t-T_0)-Q(t-T_0))}\\
&\qquad \times (E_{\mathrm{Re(Im)}}(t-T_0)\cos(W_1(t-T_0))\\
&\qquad + \sqrt{k_2}e^{1/2(G(t-T_0-\tau)-Q(t-T_0-\tau))}\\
&\qquad \times (E_{\mathrm{Re(Im)}}(t-T_0-\tau)\cos(W_2(t-T_0-\tau)))\\
&\qquad + \sqrt{k_3}e^{1/2(G(t-T_0-2\tau)-Q(t-T_0-2\tau))}\\
&\qquad \times (E_{\mathrm{Re(Im)}}(t-T_0-2\tau)\cos(W_3(t-T_0-2\tau)))
\end{aligned} \tag{8}$$

$$\begin{aligned}
&I_{\mathrm{Re-Im(Im-Re)}}\\
&\quad = +(-)\sqrt{k_1}e^{1/2(G(t-T_0)-Q(t-T_0))}\\
&\qquad \times (E_{\mathrm{Im(Re)}}(t-T_0)\sin(W_1(t-T_0))\\
&\qquad + (-)\sqrt{k_2}e^{1/2(G(t-T_0-\tau)-Q(t-T_0-\tau))}\\
&\qquad \times (E_{\mathrm{Im(Re)}}(t-T_0-\tau)\sin(W_2(t-T_0-\tau)))\\
&\qquad + (-)\sqrt{k_3}e^{1/2(G(t-T_0-2\tau)-Q(t-T_0-2\tau))}\\
&\qquad \times (E_{\mathrm{Im(Re)}}(t-T_0-2\tau)\sin(W_3(t-T_0-2\tau)))
\end{aligned} \tag{9}$$

$I_{\mathrm{Re(Im)\text{-}Re(Im)}}$ represent Re/Im parts of optical field by considering Re/Im parts of R_{i}(t) during roundtrip in ring cavity and also in both of the ring cavity and intracavity. $I_{\mathrm{Re\text{-}Re}}$ and $I_{\mathrm{Re\text{-}Im}}$ represent current dependent sources connected to the voltage node (E_{Re}) and are depend on E_{Re} and E_{Im}, respectively. Also, $I_{\mathrm{Im\text{-}Im}}$ and $I_{\mathrm{Im\text{-}Re}}$ are connected to voltage node (E_{Im}) and are depend on E_{Im} and E_{Re}, respectively.

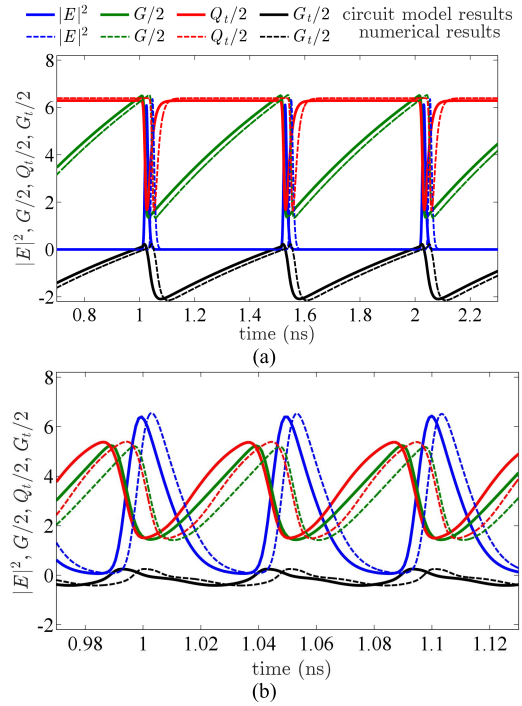

Fig. 3. Time traces of the absolute value of the normalized intensity $|E|^2$, gain G, total loss Q_t and net gain G_t for WOICS (a) H_1 and (b) H_{10}. The dashed and continuous lines indicate numerical and circuit model results, respectively.

To model (3) and (4), the saturated gain (G) and absorption (Q) are considered as node voltages. With this assumption, the terms related to the time derivations of G and Q are modeled by capacitors $C_G = \gamma_g^{-1}$, $C_Q = \gamma_q^{-1}$; respectively. Also, the first term of right side of (3) and (4) are represented by resistors $R_G = R_Q = 1$. The terms of unsaturated gain (J_g) and absorption (J_q), which are equivalent to the injection current of gain section and the reverse voltage of absorption section, are modeled by I_G and I_Q as current independent sources, respectively.

$$I_G = J_g/\gamma_g, \quad I_Q = J_q/\gamma_q \tag{10}$$

In the last terms of (3) and (4), a fraction of the G and Q are spent on amplification and attenuation of optical field. Due to the dependence of these terms on the E_{Re} and E_{Im}, current dependent sources are employed.

$$I_{DG} = \gamma_g^{-1} e^{-Q(t)}(e^{G(t)} - 1)|E(t)|^2 \tag{11}$$

$$I_{DQ} = \gamma_q^{-1} r_s e^{-Q(t)}(e^{Q(t)} - 1)|E(t)|^2 \tag{12}$$

Also, to transforms E into the output power, we define

$$P_{out} = E_{out} = |E_{\mathrm{Re}}(t) + j E_{\mathrm{Im}}(t)|^2 \tag{13}$$

The previous equations can be mapped directly into a CLM as shown in Fig. 2. P_{out} is the terminal whose node voltage models the output power. Circuit model of WOICS also can be developed using the same procedure presented for WICS circuit modeling.

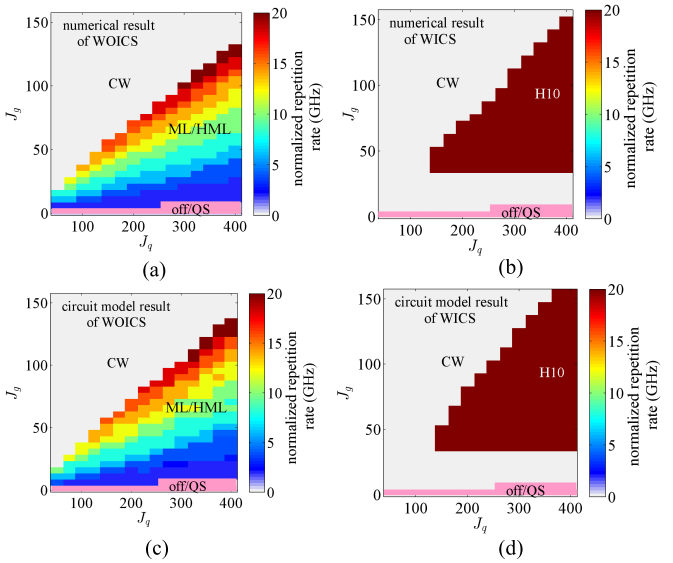

Fig. 4. Dynamic results of numerical simulation and circuit model for WOICS and WICS.

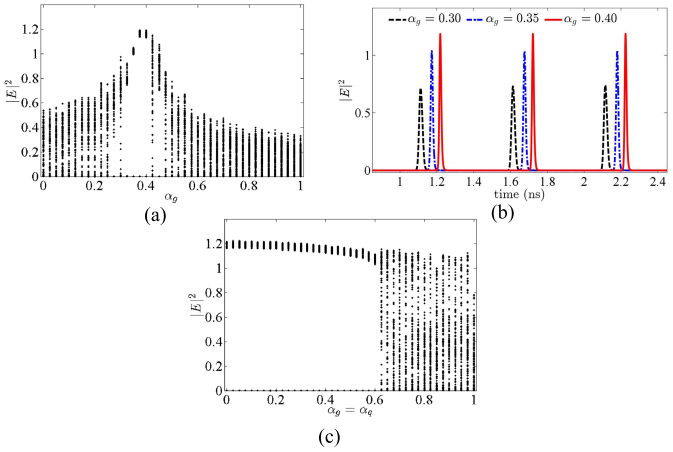

Fig. 5. (a) Extrema of the intensity time trace vs α_g, $\alpha_q = 0.40$, (b) time traces of the normalized intensity $|E|^2$ for different $\alpha_g = 0.30$, 0.35, 0.40 and $\alpha_q = 0.40$, and (c) extrema of the intensity time trace vs $\alpha_g = \alpha_q$.

IV. Results and Discussion

Fig. 3 shows time traces of the normalized intensity $|\mathrm{E}|^2$, the saturable gain G, the total loss $Q_t \equiv Q + |\ln k_0|$ and the net gain $G_t \equiv G(t) - Q_t$ for H_1 and H_{10} of WOICS. In slow stage, between two subsequent pulses, the gain and absorber media are recovered. In H_1 regime, the slow stage is longer than H_{10} regime for same J_q ($J_q = 400$), so, saturated absorption of H_1 is more compared to that of H_{10} regime. To achieve stable pulses, the experimental results indicated that the absorber medium is saturated faster than the gain one [3], Fig. 3 shows this behavior for H_1 and H_{10}. Also, Fig. 3 shows a close fit between the results of numerical analysis and circuit model.

In WOICS, all of the H_1 to H_{10} are generated with respect to fundamental frequency, i. e., 2 GHz (Fig. 4(a) and Fig. 4(c)). But in WICS, by using intracavity filter, H_{10} regime increases significantly compared to WOICS while also this regime is

more stable against the change of J_g and J_q. Additionally, H_{10} regime of WICS is generated in lower J_g and J_q. As can be seen in Fig. 4(b) and Fig. 4(d), the regimes of continuous wave (CW), Q-switching (QS), fundamental mode-locking (FML) and HML obtained by CLM have good agreement with DDE model.

The bifurcation diagram of WOICS obtained by changing the LEFs is shown in Fig. 5(a). According to Fig. 5(a) which corresponds to $\alpha_q = 0.4$, the maximum peak power of mode-locking pulses with minimum pulse width occurs when the LEFs in two sections are equal, $\alpha_q = \alpha_g$. Fig. 5(b) shows pulse train of WOICS for three different value of $\alpha_g = 0.30$, 0.35 and 0.40. The shortest pulse width is observed at $\alpha_q = \alpha_g$, and by decreasing α_g, the mode-locked pulses are broaden and therefore the peak power decreases. Finally, with further decrease in α_g, a transition from mode-locking to quasi periodic regime takes place (Fig. 5(a)). On the other hand, for $\alpha_{\mathrm{g}} > \alpha_{\mathrm{q}}$, the transition to chaotic regime occurs faster. In the case when the LEFs in the two sections are equal, by increasing LEFs, the peak power of pulses remains almost unchanged, however for $\alpha_{\mathrm{g}} = \alpha_{\mathrm{q}} > 0.6$, the transition to chaotic regime takes place (Fig. 5(c)). The results of CLM shown in Fig. 5, are in accordance with numerical simulations reported in [13].

V. Conclusion

Based on DDE, we have proposed a CLM of passively mode-locked hybrid silicon laser. Using the CLM, in fundamental and higher harmonic frequencies, we have simulated the dynamic behavior of repetition rate. The results of dynamic have demonstrated significant increase in H_{10} regime of WICS compared to WOICS. These results are validated by numerical results of DDE model. It has been also shown that using intracavity filter, the intermediate harmonics suppressed sufficiently; however, in WOICS all harmonic components are appeared. The CLM can simulate these behaviors, accurately. Additionally, the presented model predicts the effects of LEF on pulse width and peak power. The CLM and numerical results are in good agreement, and indicate that the presented CLM can be a useful engineering tool for efficient simulation and design of MLL in optoelectronic device simulators.

References

[1] M. G. Thompson, A. R. Rae, M. Xia, R. V. Penty, and I. H. White, "InGaAs quantum-dot mode-locked laser diodes," *IEEE J. Sel. Topics Quantum Electron.*, vol. 15, no. 3, pp. 661–672, May/Jun. 2009.

[2] S. Srinivasan *et al.*, "Low phase noise hybrid silicon mode-locked lasers," *Frontiers Optoelectron.*, vol. 7, no. 3, pp. 265–276, 2014.

[3] S. Arahira, Y. Matsui, and Y. Ogawa, "Mode-locking at very high repetition rates more than terahertz in passively mode-locked distributed-Bragg-reflector laser diodes," *IEEE J. Quantum Electron.*, vol. 32, no. 7, pp. 1211–1224, Jul. 1996.

[4] E. A. Avrutin, J. H. Marsh, and E. L. Portnoi, "Monolithic and multi-gigahertz mode-locked semiconductor lasers: Constructions, experiments, models and applications," *IEE Proc.-Optoelectron.*, vol. 147, no. 4, pp. 251–278, Aug. 2000.

[5] D. Arsenijević, M. Kleinert, and D. Bimberg, "Phase noise and jitter reduction by optical feedback on passively mode-locked quantum-dot lasers," *Appl. Phys. Lett.*, vol. 103, no. 23, Dec. 2013, Art. no. 231101.

[6] M. L. Davenport, S. Liu, and J. E. Bowers, "Integrated heterogeneous silicon/III–V mode-locked lasers," *Photon. Res.*, vol. 6, no. 5, pp. 468–478, 2018.

[7] S. Srinivasan *et al.*, "Harmonically mode-locked hybrid silicon laser with intra-cavity filter to suppress supermode noise," *IEEE J. Sel. Topics Quantum Electron.*, vol. 20, no. 4, pp. 8–15, Jul. 2014.

[8] M.-C. Lo, R. Guzmán, and G. Carpintero, "InP femtosecond mode-locked laser in a compound feedback cavity with a switchable repetition rate," *Opt. Lett.*, vol. 43, no. 3, pp. 507–510, Feb. 2018.

[9] H. Haus, "Theory of mode locking with a slow saturable absorber," *IEEE J. Quantum Electron.*, vol. QE-11, no. 9, pp. 736–746, Sep. 1975.

[10] L. A. Jiang, M. E. Grein, H. A. Haus, and E. P. Ippen, "Noise of mode-locked semiconductor lasers," *IEEE J. Sel. Topics Quantum Electron.*, vol. 7, no. 2, pp. 159–167, Mar. 2001.

[11] E. A. Avrutin, J. M. Arnold, and J. H. Marsh, "Dynamic modal analysis of monolithic mode-locked semiconductor lasers," *IEEE J. Sel. Topics Quantum Electron.*, vol. 9, no. 3, pp. 844–856, May 2003.

[12] J. Mulet and J. Mork, "Analysis of timing jitter in external-cavity mode-locked semiconductor lasers," *IEEE J. Quantum Electron.*, vol. 42, no. 3, pp. 249–256, Mar. 2006.

[13] A. G. Vladimirov and D. Turaev, "Model for passive mode locking in semiconductor lasers," *Phys. Rev. A, Gen. Phys.*, vol. 72, no. 3, Sep. 2005, Art. no. 033808.

[14] U. Bandelow, M. Radziunas, A. Vladimirov, B. Hüttl, and R. Kaiser, "40 GHz mode-locked semiconductor lasers: Theory, simulations and experiment," *Opt. Quantum Electron.*, vol. 38, nos. 4–6, pp. 495–512, Mar. 2006.

[15] S. Meinecke, L. Drzewietzki, C. Weber, B. Lingnau, S. Breuer, and K. Lüdge, "Ultra-short pulse generation in a three section tapered passively mode-locked quantum-dot semiconductor laser," *Sci. Rep.*, vol. 9, no. 1, pp. 1–14, Dec. 2019.

[16] M. Radziunas, A. G. Vladimirov, E. A. Viktorov, G. Fiol, H. Schmeckebier, and D. Bimberg, "Pulse broadening in quantum-dot mode-locked semiconductor lasers: Simulation, analysis, and experiments," *IEEE J. Quantum Electron.*, vol. 47, no. 7, pp. 935–943, Jul. 2011.

[17] C. Otto, K. Lüdge, A. G. Vladimirov, M. Wolfrum, and E. Schöll, "Delay-induced dynamics and jitter reduction of passively mode-locked semiconductor lasers subject to optical feedback," *New J. Phys.*, vol. 14, no. 11, Nov. 2012, Art. no. 113033.

[18] M. Shekarpour and M. H. Yavari, "Proposal of phase noise and jitter reduction in long-ring hybrid silicon mode-locked laser by intra-cavity reflectors," *Opt. Lett.*, vol. 46, no. 12, pp. 2904–2907, 2021.

[19] M. Shekarpour and M. H. Yavari, "Jitter reduction of mode-locked hybrid silicon laser with intra cavity filter," in *Proc. Int. Conf. Numer. Simulation Optoelectron. Devices (NUSOD)*, Sep. 2020, pp. 75–76.

[20] M. Shekarpour and M. H. Yavari, "Super mode noise suppression of silicon hybrid mode-locked ring laser using a symmetric Fabry–Pérot filter," *J. Opt. Soc. Amer. B, Opt. Phys.*, vol. 39, no. 2, pp. 527–534, 2022.

[21] M. Shekarpour and M. H. Yavari, "Timing jitter reduction of silicon hybrid harmonically mode-locked ring laser using an integrated sampled-grating DBR," *Opt. Lett.*, vol. 47, no. 8, p. 2016, Apr. 2022, doi: 10.1364/OL.452246.

[22] L. Chrostowski *et al.*, "Design methodologies for silicon photonic integrated circuits," *Proc. SPIE*, vol. 8989, Mar. 2014, Art. no. 89890G.